



Neil C. Rogers

Neil C. Rogers<sup>1</sup>, Alasdair Helliwell<sup>2</sup> and Karl Atkinson<sup>3</sup>

1: Space & Planetary Physics group, University of Lancaster, UK  
2: Airbus Defence & Space, Portsmouth, Hampshire, UK 3: Airbus Defence & Space, Stevenage, Hertfordshire, UK  
n.rogers1@lancaster.ac.uk

## 1: Introduction

In 2021 the European Space Agency (ESA) will launch the Biomass satellite, a synthetic aperture radar (SAR) to measure the distribution of biomass density in the world's forests. Its low operating frequency,  $f = 435$  MHz enhances foliage and ground penetration of the radio waveform but also amplifies ionospheric scintillation (scattering from irregularities) and Faraday rotation (FR). The Biomass SAR will be fully polarimetric, transmitting and receiving radar chirps in orthogonal (H and V) planes. One possible option for the on-orbit calibration of the H and V transmit/receive channels (determining cross-talk and channel imbalances) is to locate the ground-based transponder near the geomagnetic equator so as to reduce two-way FR to a level equivalent to the system cross-talk requirement.

This poster describes how models of ionospheric electron density and predictions of the future geomagnetic field are combined with the geometry of the radar beam and the sun-synchronous orbit to select candidate transponder sites with a two-way FR of less than 1.8° (equivalent to a cross-talk of -30 dB).

## 2: Modelling Ionospheric Faraday Rotation (FR)

To a first-order approximation, the one-way FR (in radians) is

$$\Omega \approx \frac{e^3}{8\pi^2 \epsilon_0 m^2 c} \frac{B \cos(\psi)}{f^2} \int N_e ds \quad (\text{Eqn 1})$$

Constant = 23,648 A m<sup>2</sup> kg<sup>-1</sup>      Total Electron Content (TEC) (electron density integrated over ray path)

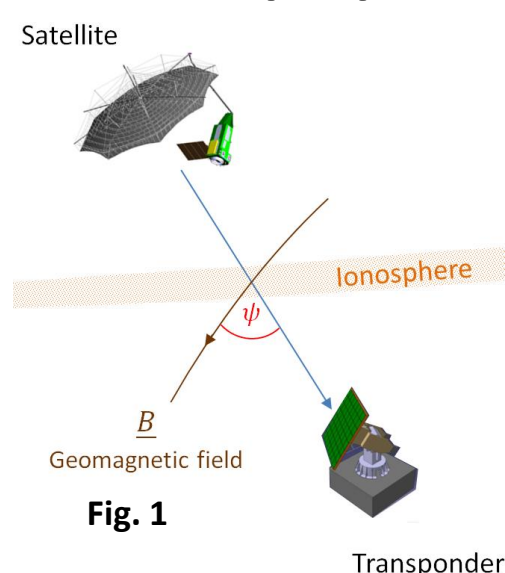


Fig. 1

The geomagnetic field,  $B$ , is determined from the International Geomagnetic Reference Field (IGRF) [1], with secular (long-term) variations extrapolated linearly to cover the mission years c.2021-2026. Electron density,  $N_e$ , is from the NeQuick2 climatological model [2]. Since the orbit is sun-synchronous, the Universal Time input parameter for NeQuick2 is calculated from the satellite location noting whether the satellite is ascending (near dawn) or descending (near dusk).

The angle  $\psi$  between  $B$  and the radio ray path (see Fig. 1) is calculated from the ionospheric pierce point location, look-angle (i.e. the satellite-zenith angle at the ground transponder), satellite heading and the satellite's yaw steer angle.

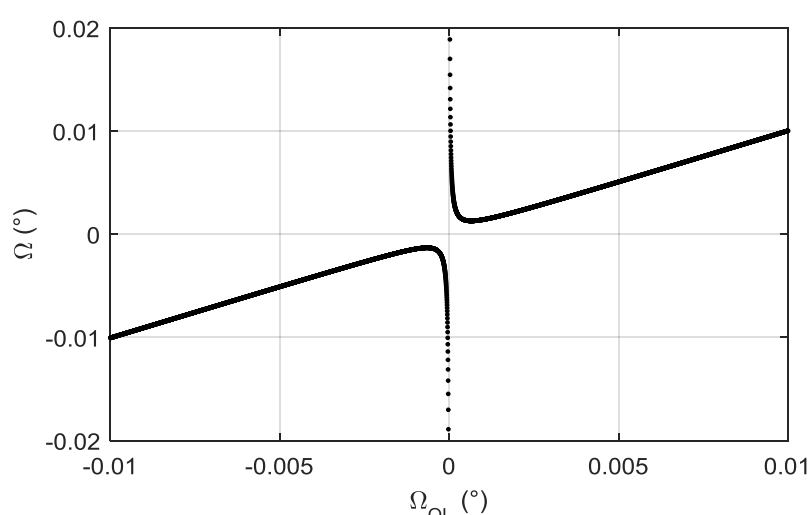


Fig. 2. Corrected FR ( $\Omega$ ) (ordinates) (from [3]) vs the approximate form in Eqn 1 (abscissae) for typical values of  $B = 0.2$  G and  $TEC = 10$  TECU.

Discrepancies from the approximate form for  $\Omega$  arise only where absolute FR < 0.001° as shown in Fig. 2.

Table 1. Model Parameters

Years	2014, 2019, 2024
Dates	21 Mar., 21 Jun., 21 Sep., 21 Dec.
Sunspot number	63 (median), 106 (upper quartile)
Effective height of ionosphere	350 km
Height of satellite	666 km
Local Time of Ascending Node	06:00
Orbit inclination	98° (sun-synchronous)
Beam look direction (azimuth)	Left-looking (90°)
Look angles (°) – Swath 1	20.7, 22.7, 24.6
Look angles (°) – Swath 2	24.2, 26.0, 27.7
Look angles (°) – Swath 3	27.3, 28.7, 30.0

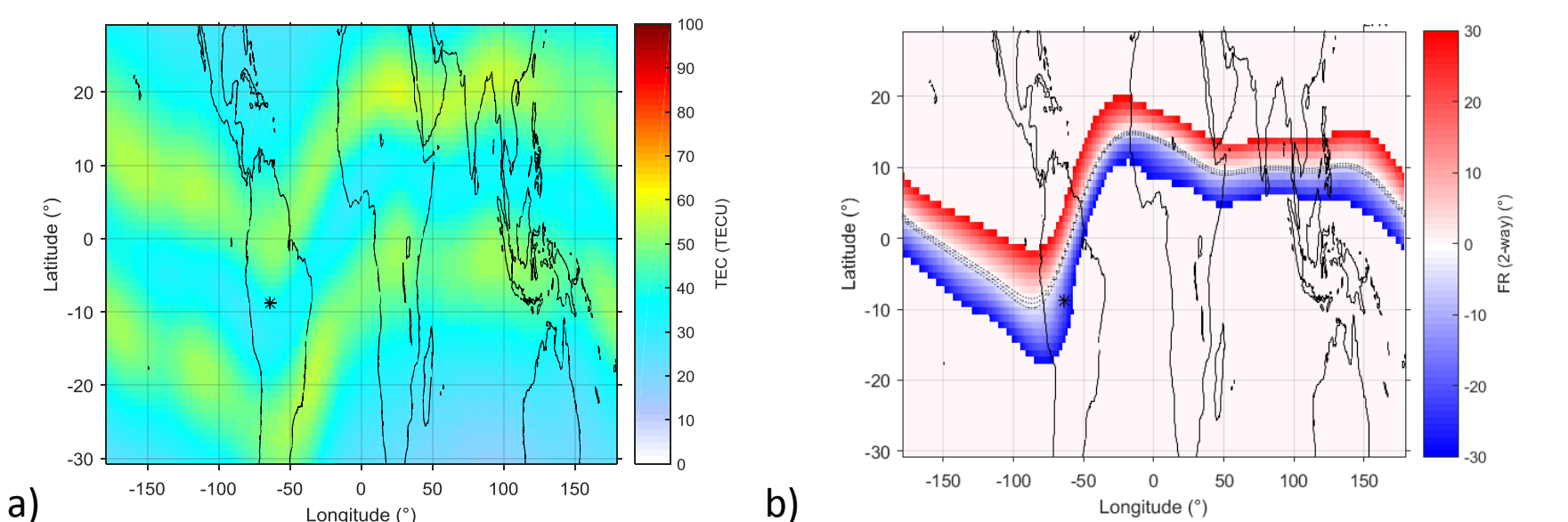


Fig. 3. a) Total Electron Content (TEC) and b) FR predictions for the descending (dusk-side) satellite. (21/3/2019, Sunspot number = 106, Look-angle=25.95°) ±1.8° FR contours are shown as dotted lines in panel (b).  $|FR| > 30^\circ$  is not shown (at higher latitudes). Zero-Doppler yaw steering is applied (as explained below).

## 3: The Effect of Zero-Doppler Steering on FR

Variations of the Doppler centroid (see Fig. 4) cause errors in azimuth compression, range migration correction, geolocalisation, and phase errors in interferometric image pairs (in case of coregistration errors). The satellite may minimise the Doppler centroid by applying yaw rotation of [4]

$$\psi_{ZD} = \tan^{-1} \left( \frac{\sin(i) \cos(u)}{N_{revs} - \cos(i)} \right) \quad (\text{Eqn 2})$$

where  $N_{revs}$  = number of satellite orbits per day,  $i$  = orbit inclination (98°),  $u$  = argument of latitude. This affects the angle  $\psi$  in Eqn 1 and hence changes FR, shifting the 0° FR contour (see Fig. 3b) by typically 1° in latitude.

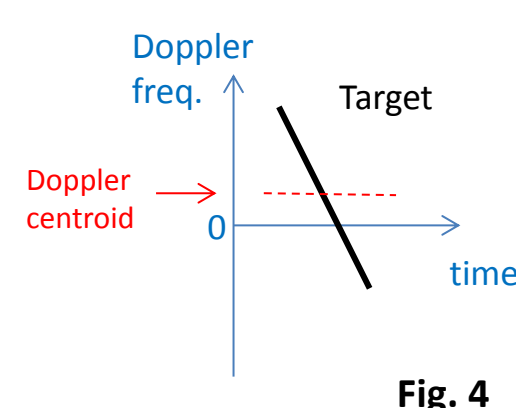


Fig. 4

## References

[1] Thébaud, E., C. C. Finlay, C. D. Beggan, P. Alken, J. Aubert, et al. (2015) Earth, Planets and Space, 67, 79. DOI: 10.1186/s40623-015-0228-9

[2] Nava, B., P. Coisson, and S.M. Radice (2008), J. Atmos. Solar-Terr. Phys., 70(15), DOI: 1856–1862.10.1016/j.jastp.2008.01.015.

[3] Hudson, R.M. (1969), Planet Space Sci., 17, 1045–1050, DOI: 10.1016/0032-0633(69)90109-3.

[4] Fiedler, H., E. Boerner, J. Mittermayer, and G. Krieger (2005), IEEE Geosci. Remote Sens. Lett. 2(2), DOI: 10.1109/LGRS.2005.844591.

## 4: Zero-FR Steering

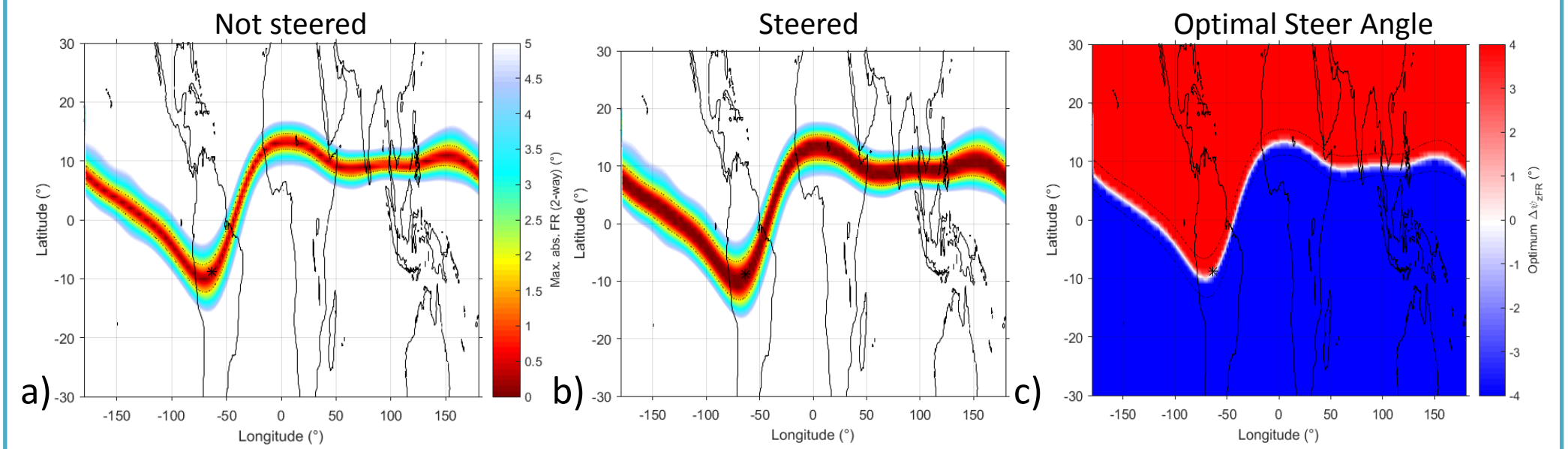


Fig. 5. a) Max. abs. FR (no additional yaw steer), b) Max. abs. FR with optimal yaw steer in the range  $\psi_{ZFR} = [-4^\circ, \dots, +4^\circ]$ . c) Optimal values of  $\psi_{ZFR}$ . (Max. values for ascending satellite, all 9 look angles, 4 seasons (2019), Sunspot no.: 106, Zero-Doppler steering applied.)

Fig. 5 demonstrates how the absolute FR angle may be optimised by applying an additional satellite yaw steer in the range  $[-4^\circ, \dots, +4^\circ]$ . This has the effect of expanding the latitude region of low FR (compare panels (b) (yaw steered) and (a) (not steered)). However, the optimal steer angles (panel (c) indicate a rapid ( $\sim 0.5^\circ/s$ ) steer would be required as the satellite crosses the geomagnetic equator.

## 5: Radar Transponder Site Selection

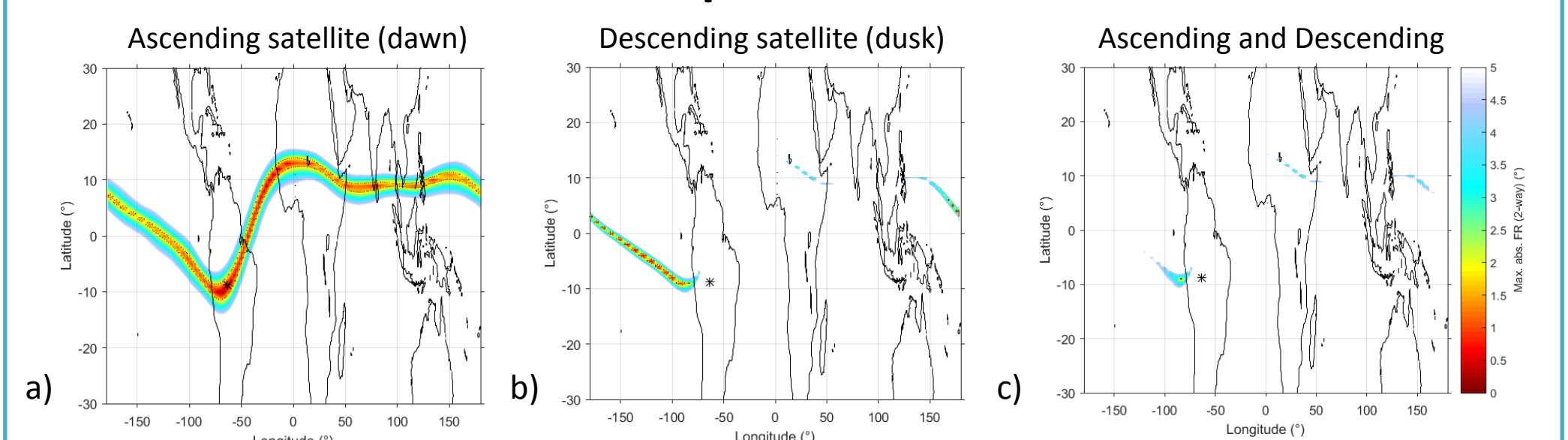


Fig. 6. Max. abs. FR for (a) Ascending satellite, (b) Descending satellite and (c) both. Max. values for ascending satellite, all 9 look angles, 4 seasons (2019), Sunspot number: 106, Zero-Doppler steering applied.)

Fig. 6 presents an example of the “worst case” max. abs. FR angles predicted for a) the ascending (dawn side) satellite, b) the descending satellite and c) both. The number of locations suitable for calibration on descending satellites is very limited.

Seven candidate locations were selected (see map, Fig. 7). FR predictions are presented as a function of look angle in Fig. 8 for a) Site A in Brazil, and b) Site B in Peru, for the ascending satellite. Site A is favourable due to consistently low FR and a low gradient of FR with look angle.

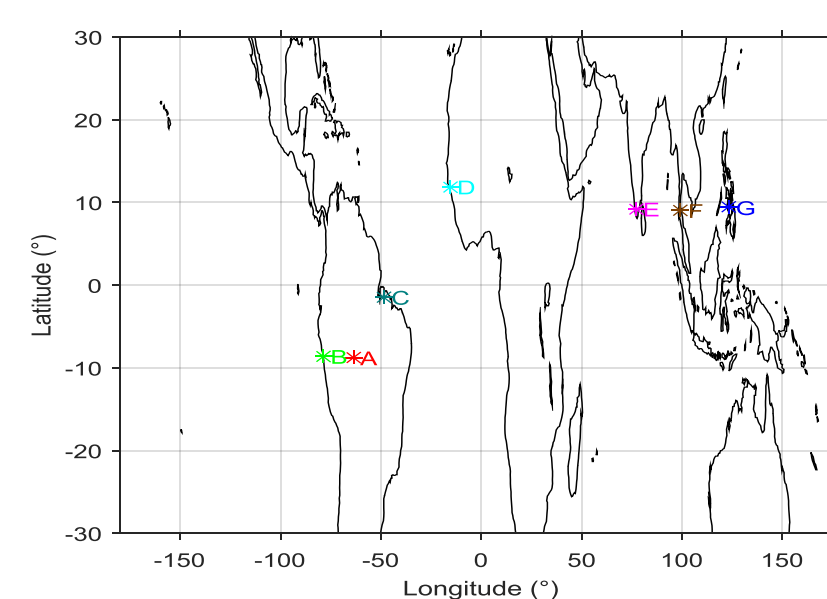


Fig. 7. Seven candidate transponder locations.

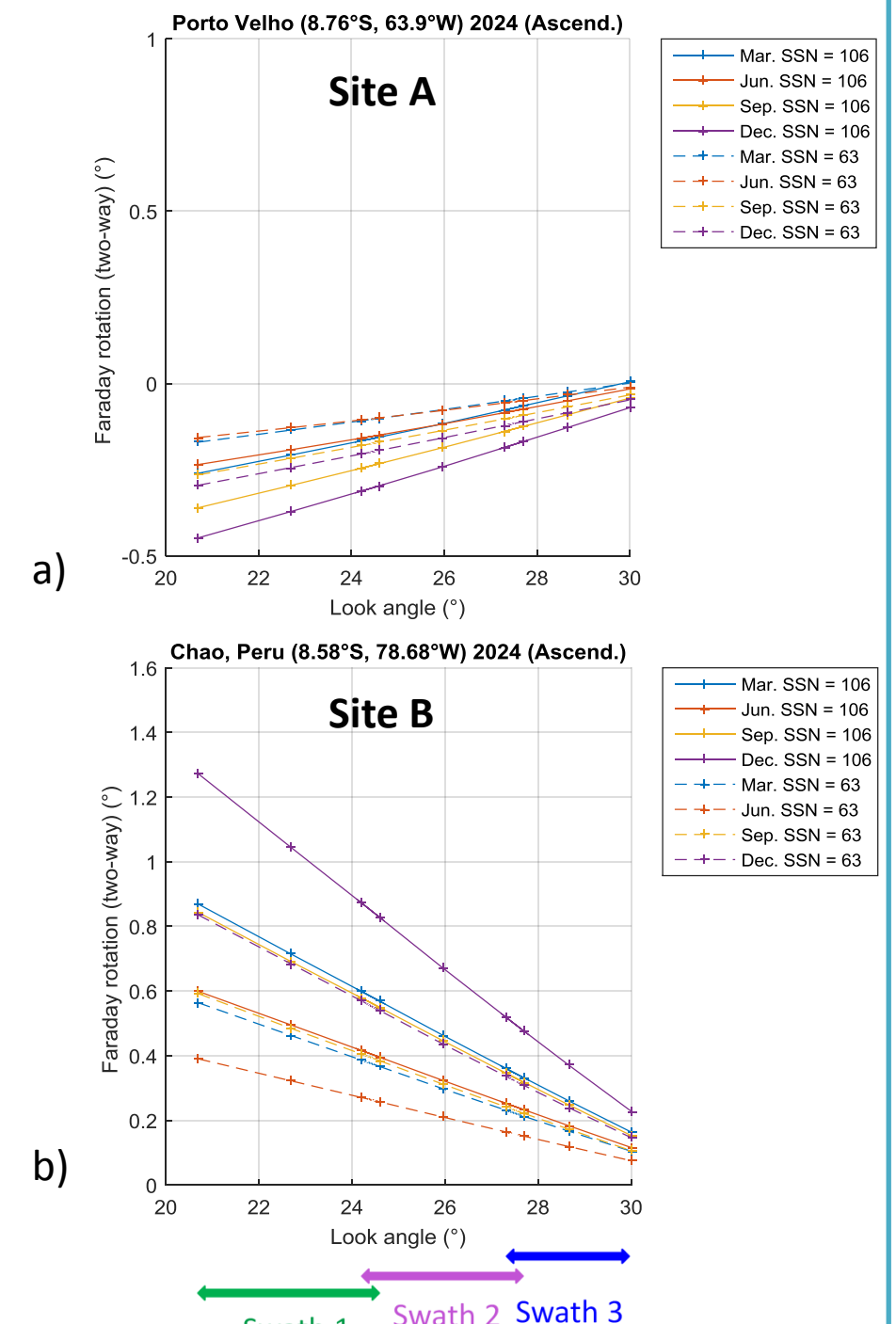


Fig. 8. FR predictions for a) Site A and b) Site B, for the ascending satellite in year 2024.

## 6: Conclusions

- Faraday Rotation has been modelled and mapped globally for a sun-synchronous side-looking satellite radar. The model is adaptable for a range of satellite beam steer angles and orbit geometries. Simulations for the 2021-2026 ESA Biomass radar mission predict that
- FR (and TEC) will be smallest on dawn side (i.e. for the ascending satellite) (cf. Dusk).
- FR changes with the seasons but the 0° FR contour is relatively unchanged.
- Zero-Doppler steering shifts the 0° FR contour by  $\sim 1^\circ$  latitude.
- “Zero-FR” steering
  - Expands the latitude band for which abs. FR < 1.8° and reduces the minimum value within that band
  - But requires a rapid yaw steer as the satellite crosses the geomagnetic equator
- Of seven candidate transponder sites studied, Site A (Porto Velho, Brazil) is recommended:
  - It has the lowest FR (< 0.5° for all swaths and throughout the mission years)
  - It has the lowest gradient of FR with look-angle.
  - But it is suitable for calibration on ascending (dawn side) only.

## Acknowledgement

This work was funded by the European Space Agency.

